

See discussions, stats, and author profiles for this publication at: <http://www.researchgate.net/publication/14291131>

High resolution measurement of cerebral blood flow using intravascular tracer bolus passages. Part I: Mathematical approach and statistical analysis

ARTICLE *in* MAGNETIC RESONANCE IN MEDICINE · NOVEMBER 1996

Impact Factor: 3.4 · DOI: 10.1002/mrm.1910360510 · Source: PubMed

CITATIONS

951

DOWNLOADS

156

VIEWS

256

5 AUTHORS, INCLUDING:



[Leif Østergaard](#)

Aarhus University

238 PUBLICATIONS 7,949 CITATIONS

SEE PROFILE

High Resolution Measurement of Cerebral Blood Flow using Intravascular Tracer Bolus Passages. Part I: Mathematical Approach and Statistical Analysis

Leif Østergaard, Robert M. Weisskoff, David A. Chesler, Carsten Gyldensted, Bruce R. Rosen

The authors review the theoretical basis of determination of cerebral blood flow (CBF) using dynamic measurements of nondiffusible contrast agents, and demonstrate how parametric and nonparametric deconvolution techniques can be modified for the special requirements of CBF determination using dynamic MRI. Using Monte Carlo modeling, the use of simple, analytical residue models is shown to introduce large errors in flow estimates when actual, underlying vascular characteristics are not sufficiently described by the chosen function. The determination of the shape of the residue function on a regional basis is shown to be possible only at high signal-to-noise ratio. Comparison of several nonparametric deconvolution techniques showed that a nonparametric deconvolution technique (singular value decomposition) allows estimation of flow relatively independent of underlying vascular structure and volume even at low signal-to-noise ratio associated with pixel-by-pixel deconvolution.

Key words: cerebral blood flow (CBF); dynamic magnetic resonance imaging (MRI); nonparametric deconvolution; susceptibility contrast.

INTRODUCTION

One of the main goals of functional NMR is noninvasive, high resolution determination of cerebral perfusion. With the development of rapid MR imaging sequences, dynamic imaging of concentration time curves after bolus-injection of purely intravascular contrast agents has become possible on time scales comparable with vascular mean transit times (MTT). Using the central volume theorem (1, 2), these concentration time curves have been used to calculate regional cerebral blood volume (rCBV) using CT (3) and, more recently, MRI (4, 5). Attempts have been made to use bolus passages of intravascular contrast agents to calculate regional CBF (6–8) and myo-

cardial perfusion (9). This technique involves knowledge of vascular structure through the *residue function*, determining how the observed tracer is retained in the vasculature. This has caused some to reject this as a method of determining blood flow since the vascular structure is not known *a priori* (10), whereas others have pursued mathematical and numerical deconvolution approaches to determine both flow and the necessary characteristics of the vascular bed *a posteriori* from measurements (model independent approaches) (7, 8). The latter approach in turn may provide important information about the microvasculature. Other authors have proposed general analytical models to describe the shape of the residue function (model dependent approaches) (11).

In this study we seek to determine a robust mathematical approach to determine flow and vascular tracer retention by deconvolution of dynamic MRI tissue concentration curves with noninvasively determined arterial input curves. We first review the theory and inherent mathematical problems of flow measurements with nondiffusible tracers. Two main categories of nonparametric deconvolution techniques are described and modified for use with MRI determination of rCBF. We then use Monte Carlo simulations to address the possibilities of determining the shape of the vascular residue function using nonparametric deconvolution techniques. Finally, we analyze the errors on the estimated CBF values that may be involved in (i) using simple, analytical expressions to describe the vascular residue function and (ii) using nonparametric deconvolution techniques at signal-to-noise ratios (SNR) typical of dynamic MRI experiments.

THEORY

We briefly review the definitions of the MTT, CBV, and CBF as well as their inter-relationship given by the central volume theorem (1, 2). Given these definitions, we state and discuss the central equation in our approach to the determination of CBF using nondiffusible, paramagnetic MRI tracers.

Consider a bolus of nondiffusible tracer given at time $t = 0$ in the feeding vessel(s) to a volume of interest (VOI) of tissue. The individual particles of the tracer follow different paths through the VOI and their transit times thus have a distribution characteristic of the flow and the vascular structure. The probability density function of these transit times is denoted $h(t)$, the *transport function*. When an arterial input $C_a(t)$ is given to the VOI, the concentration of tracer in the venous output, $C_v(t)$, from

MRM 36:715–725 (1996)

From the MGH-NMR Center, Department of Radiology, Massachusetts General Hospital, Harvard Medical School, Charlestown, Massachusetts; and the Department of Neuroradiology (L.Ø., C.G.) and PET-Center (L.Ø.), Århus University Hospital, Århus, Denmark.

Address correspondence to: Leif Østergaard, M.D., M.S., Department of Neuroradiology, Århus Kommunehospital, Nørrebrogade 44, DK-8000 Århus, Denmark.

Received July 27, 1995; revised January 31, 1996; accepted May 9, 1996.

This work was supported by The Danish Research Academy (S940197), The Danish Medical Research Council (12-1634-1, 1993), Danish Physicians' Insurance (under the auspices of Codan Insurance Company, Copenhagen), The Einar Willumsen Memorial Foundation, The King Christian 10th Foundation, The Beckett Foundation, by Public Health Service Grants RO1-CA40303, RO1-HL39810, the Whitaker Foundation RO1-CA66072, and PO1-CA48729.

0740-3194/96 \$3.00

Copyright © 1996 by Williams & Wilkins

All rights of reproduction in any form reserved.

the region is thus given by

$$C_V(t) = C_a(t) \otimes h(t) \equiv \int_0^t C_a(\tau)h(t - \tau)d\tau \quad [1]$$

where \otimes denotes convolution. The MTT for the tracer particles is defined in terms of the density function:

$$\text{MTT} \equiv \frac{\int_{-\infty}^{\infty} \tau h(\tau)d\tau}{\int_{-\infty}^{\infty} h(\tau)d\tau} \quad [2]$$

This equation has been used to determine flow under different assumptions about the relationship between MTT and the observed passage time of an intravascular contrast bolus (6). As pointed out by Weisskoff *et al.* (12), the distinction between this MTT and the first moment of the concentration time curve obtained from imaging of intravascular bolus passages is, however, crucial in attempts to measure absolute flow using intravascular tracers.

The amount of intravascular tracer in the VOI is determined by

$$\text{CBV} = \frac{\int_{-\infty}^{\infty} C_{\text{VOI}}(\tau)d\tau}{\int_{-\infty}^{\infty} C_a(\tau)d\tau} \quad [3]$$

In the case of brain tissue with an intact blood brain barrier (BBB), the distribution space of common paramagnetic NMR contrast agents is equal to the intravascular, extracellular space, i.e., the plasma volume. The fraction of tissue available for tracer distribution is thus $(1 - \text{Hct}_m) \cdot \text{CBV}_f$, where Hct_m is the microvascular hematocrit and CBV_f is the cerebral full blood volume. Hct_m is a complicated function of vessel size, flow, and pathophysiological conditions but is generally 40–100% of the systemic blood hematocrit (13). The discussion of these effects is outside the scope of this paper. Throughout our simulations, values of CBF and CBV will refer to full blood flow, assuming a macrovascular to microvascular hematocrit ratio of 2/3 (13), independent of flow.

With the definition of MTT and CBV above, the central volume theorem (1, 2) states that the relationship between these and tissue flow, F_t

$$\text{MTT} = \frac{\text{CBV}}{F_t} \quad [4]$$

The central quantity in bolus-passage experiments is the fraction of injected tracer still present in the vasculature at time t , described by the *residue function* $R(t)$,

$$R(t) \equiv \left[1 - \int_0^t h(\tau)d\tau \right] \quad [5]$$

Note that by the definition of $h(t)$ as a probability density function, $R(0) = 1$ and $R(t)$ is a positive, decreasing function of time.

The concentration $C_{\text{VOI}}(t)$ of tracer within a given VOI can now be written

$$C_{\text{VOI}}(t) = F_t \int_0^t C_a(\tau)R(t - \tau)d\tau \quad [6]$$

Equation [6] is the central equation in our approach to determine flow using nondiffusible tracers. It states that the initial height of the deconvolved concentration time curve equals the flow, F_t . It is important to note that the arterial input function in Eq. [6] may undergo dispersion during its passage from the point of measurement to more peripheral tissue. This dispersion can be described mathematically as a convolution with a vascular transport function $h^*(t)$ (cf. Eq. [1]). If the residue function determined by using an arterial input that is subsequently dispersed is denoted $R^*(t)$ and the “true” residue function $R(t)$, using Eq. [6] would consequently yield $R^*(t) = h^*(t) \otimes R(t)$. The initial height of the deconvolved curve will thus be underestimated by the spread in $R^*(t)$. This underlines the importance of measuring the arterial input values close to the observed tissue to avoid dispersion.

Equation [6] is not straight forward to solve for F_t , because $R(t)$ is an unknown function dependent on local vascular structure (10). This type of so-called *inverse problems* (14, 15), where integral equations are solved with respect to an unknown kernel, appears frequently in the biomedical literature, mainly in the context of venous output measurements (Eq. [1]). The basic principles in solving these equations are, however, generally applicable and in the following we will apply and refer to them in the context of vascular residue functions.

The approaches to deconvolve Eq. [6] are divided into two main categories. In *model dependent techniques*, we assume a specific analytical expression or the shape of $R(t)$. Assuming a specific shape for $R(t)$ imposes assumptions on the tissue microvasculature. For this reason, some have argued that Eq. [6] cannot be used to determine flow by deconvolution with an arterial input function in part since $R(t)$ cannot be known *a priori* with sufficient precision (10). This problem can, at least in theory, be circumvented by performing nonparametric deconvolution without *a priori* knowledge of $R(t)$. The latter *model independent* approach, where the flow and the shape of $R(t)$ are determined from the experiment by nonparametric deconvolution, forms the other main category of approaches to solve Eq. [6] for F_t and $R(t)$.

The goal of this work was to find the optimal deconvolution approach to allow determination of $R(t)$ and tissue flow from Eq. [6]. In the following, we describe how we modified and compared general model-dependent as well as model-independent approaches for the special requirements of CBF measurements using nondiffusible susceptibility tracers in MRI.

DECONVOLUTION TECHNIQUES

Model-Dependent (Analytical) Deconvolution

One reason for describing $R(t)$ with an analytical function is partly that it makes the deconvolution in Eq. [6] more stable since it reduces the degrees of freedom for the resulting shape or the shape of $R(t)$. To clarify the division of approaches in this paragraph, we use the term “deconvolution” to describe the determination of CBF and MTT from arterial and tissue concentration time curves by nonlinear least squared fitting, although this terminology should perhaps be reserved for the model-dependent approaches below. This approach introduces the assumption that the actual vascular structure can be described by a particular function.

Exponential decrease has been proposed as a general model for tissue residue functions. This is based on a simple model of the vascular bed as one single, well-mixed compartment. For such a system, the residue function is an exponential (16, 17). Taking into account more complicated models of capillaries including the effects of “plug” flow (the fact that the red blood cells fill the capillary lumen completely and thus to some extent prevent mixing), it has been argued that a linear combination of a finite number of exponentials still may be an appropriate model for the residue function (11).

We used a single exponential as a first-order model to describe the residue function:

$$R(t, \text{MTT}) = e^{-\frac{t}{\text{MTT}}} \quad [7]$$

We used general nonlinear least squared minimization to fit for MTT and F_t (15).

Model-Independent (Nonparametric) Deconvolution

In this approach, $R(t)$ is determined along with F_t . Equations [1] and [6] are, with respect to $R(t)$, both Fredholm integral equations of the first kind (14, 15). These equations are generally unstable in the sense that infinitesimal changes (in our case noise) in $C_{\text{VOI}}(t)$ give rise to finite changes in $R(t)$. The techniques described below mainly differ in the way they moderate the effects of noise in the measurements. The techniques fall into two subcategories: In the first, *transform* approach, the convolution theorems for the Fourier, Z , or Laplace transforms are used to deconvolve Eq. [6]. In the second, *algebraic* approach, Eq. [6] is rewritten as a matrix equation and solved.

These techniques have mainly been applied at high SNR to find residue or transport functions with long MTTs compared with the temporal resolution of the experiments. In the following, we will focus on modifications necessary for our applications, finding CBF using dynamic MRI of bolus passages.

Transform Approach. In this approach, the convolution theorem of the Laplace, Z , or Fourier transform (FT) is used (7, 8, 18–21). Denoting by $F\{\}$ the Fourier transform (FT), the convolution theorem states that $F\{\}$ is multiplicative to convolution. Equation [6] thus becomes:

$$F\{C_{\text{VOI}}(t)\} = F_t \cdot F\{C_a(t)\} \otimes R(t) = F_t \cdot F\{C_a(t)\} \cdot F\{R(t)\} \quad [8]$$

or in other words,

$$R(t) = F_t^{-1} F^{-1} \left\{ \frac{F\{C_{\text{VOI}}(t)\}}{F\{C_a(t)\}} \right\} \quad [9]$$

where $F^{-1}\{\}$ denotes the inverse FT. The residue function and flow can thus be determined by taking the inverse FT of the ratios of two transforms at every time point of the known arterial input and tissue time-activity curve. This approach is—in this form—very sensitive to noise. The FT of the arterial and cerebral curves, however, yield a frequency representation of the data where noise is represented at high frequencies, whereas “real” physiological signal has higher power at lower frequency. This allows one in principle to apply a filter that retains “physiological” frequencies but damps noise before performing the inverse Fourier transform to determine $F_t \cdot R(t)$. We implemented an automated filtering procedure described by Gobbel and Fike (7), which is a modified version of the Wiener filter (15), increasing the strength of the filter until a global constraint on the degree of oscillations was fulfilled. Rempp *et al.* (8) also reported using an optimal Wiener filter for deconvolution of tissue concentration time curves to determine flow.

Algebraic Approach. This approach is based on an algebraic reformulation of the convolution integrals in Eqs. [1] and [6] and has been used extensively in the analysis of tracer transport functions (22–26).

Assume that the arterial and cerebral concentrations are measured at a set of equally spaced time points t_1, t_2, \dots, t_N . Assume that, over small time intervals t , the residue function and arterial input values are constant. The convolution in Eq. [6] can then be formulated as a matrix equation (22):

$$C(t_i) = \int_0^{t_i} C_a(\tau) R(t - \tau) d\tau \approx \Delta t \sum_{i=0}^j C_a(t_i) R(t_j - t_i) \quad [10]$$

or

$$\Delta t \begin{pmatrix} C_a(t_1) & 0 & \dots & 0 \\ C_a(t_2) & C_a(t_1) & \dots & 0 \\ \dots & \dots & \dots & \dots \\ C_a(t_N) & C_a(t_{N-1}) & \dots & C_a(t_1) \end{pmatrix} \cdot \begin{pmatrix} R(t_1) \\ R(t_2) \\ \dots \\ R(t_N) \end{pmatrix} = \begin{pmatrix} C_{br}(t_1) \\ C_{br}(t_2) \\ \dots \\ C_{br}(t_N) \end{pmatrix} \quad [11]$$

In the following we shall use the short-hand vector notation

$$\mathbf{A} \cdot \mathbf{b} = \mathbf{c} \quad [12]$$

for this equation, where \mathbf{b} contains the elements of $R(t_i)$, $i = 1, 2, \dots, N$, and \mathbf{c} are the measured cerebral tracer concentrations (22–26). Note that Eq. [11] can be solved iteratively for the elements of \mathbf{b} . This approach is, however, extremely sensitive to noise, causing $R(t)$ to oscillate. Solving Eq. [12] thus involves minimizing the effects of noise and at the same time minimizing

$$\|\mathbf{A} \cdot \mathbf{b} - \mathbf{c}\| \quad [13]$$

where $\|\cdot\|$ denotes the vector norm.

The algebraic approach has been used extensively in the analysis of tracer transport functions and residue functions in organs with relatively long MTTs. The technique assumes that arterial and tissue concentrations are constant between measurements. In the context of rCBF measurements using dynamic MR imaging of intravascular bolus passages, both the arterial input function and the residue function are expected to vary over small time scales compared with the temporal resolution of the measurements (1–1.5 s for typical spin-echo EPI imaging). The constancy of these functions between measurements is thus a poor approximation. In our approach we assumed that $C_a(t)$ and $R(t)$ both vary *linearly* with time. It can be shown that the elements a_{ij} of the matrix A in Eq. [11] become

$$a_{ij} = \begin{cases} \Delta t(C_a(t_{i-j-1}) + 4 \cdot C_a(t_{i-j}) + C_a(t_{i-j+1}))/6 & 0 \leq j \leq i \\ 0 & \text{else} \end{cases} \quad [14]$$

In our work, then, this matrix was used for A when solving Eq. [13].

Regularization. A widely used approach to solve Eq. [13] is *regularization*, minimizing

$$|A \cdot \mathbf{b} + \mathbf{f}(\mathbf{b}) - \mathbf{c}| \quad [15]$$

rather than Eq. [13], where $\mathbf{f}(\mathbf{b})$, the regularization term, is a function of \mathbf{b} . By appropriately choosing \mathbf{f} , the solution \mathbf{b} can be constrained to be mathematically “well-behaved” and at the same time be physiologically meaningful. Regularization, in a biological context, has mainly been applied to determine transport functions (cf. Eq. [1]). Existing regularization approaches are thus not applicable for our purpose, determining residue function. The major drawback of regularization is that, like analytical deconvolution, it creates a result that matches *a priori* expectations of the shape of \mathbf{b} at the expense of the the quality of the fit to the actual data (15).

We implemented a regularization term modified for finding residue functions without significantly affecting the fit to experimentally determined data. The regularization term $\mathbf{f}(\mathbf{b})$ imposes a mild constraint on $R(t)$ of being a decreasing function of time:

$$f_j(\mathbf{b}) = \begin{cases} P_{\text{REG}} \cdot (b_j - b_{j-1}) & \text{if } b_j < 1.1 \cdot b_{j+1} \\ 0 & \text{else} \end{cases} \quad [16]$$

where P_{REG} is a free parameter. Increasing P_{REG} 's size allows one to strengthen the constraint on $R(t)$ of being a decreasing function of time relative to that of solving Eq. [9]. This regularization term has the advantage of disappearing when $R(t)$ is a decreasing function of time and thus will not affect the quality of the fit as long as this single physiological constraint is fulfilled. We solved Eq. [15] for the elements of $R(t_i)$ by least squared minimization (15).

Singular Value Decomposition (SVD). Another technique to solve Eq. [12] uses the SVD. Apart from changing the matrix A in Eq. [11] for the use with rapidly varying functions of time, we did not modify the SVD technique. We will thus restrict ourselves to a brief general description of the technique.

The SVD constructs matrices V , W , and U^T so that the inverse of A in Eq. [12], A^{-1} , can be written:

$$A^{-1} = V \cdot W \cdot U^T \quad [17]$$

where W is a diagonal matrix (i.e., off-diagonal elements are zero). V and U^T are orthogonal and transpose orthogonal matrices (i.e., have orthogonal, unit length columns), respectively. Given this inverse matrix, \mathbf{b} , and consequently $R(t)$, is found simply as

$$\mathbf{b} = V \cdot W \cdot (U^T \cdot \mathbf{c}) \quad [18]$$

The main force of the SVD is that the diagonal elements in W are zero or close to zero corresponding to linear equations in Eq. [11] that are close to being linear combinations of each other. This fact thus allows one to identify elements in the matrix A that causes the solution \mathbf{b} to oscillate or otherwise be meaningless in a biomedical modeling context. In terms of sampling data from bolus passage experiments, the fact that equations in Eq. [11] are close to being linear combinations of each other means that data are being sampled at time points where changes in arterial or cerebral concentration time curves over time are small relative to the noise. By eliminating (setting equal to zero) diagonal elements below a certain threshold in W , one can consequently minimize these effects before calculating \mathbf{b} . The resulting \mathbf{b} (after elimination of diagonal elements) can be shown to be the best possible solution of Eq. [13] in a least squared sense (15). For more detail, see Press *et al.* (15) and Van Huffel *et al.* (26) and references therein.

SIMULATION SCHEME

We performed a series of Monte Carlo simulations to determine the performance of the deconvolution techniques under different physiological characteristics and SNRs. We first describe the arterial input and the physiological characteristics of the vascular bed used in our simulations, and then describe how the nonparametric deconvolution techniques used were optimized at each SNR before our simulations.

Simulated Arterial Input

For our simulations, we used an arterial input with a shape and size that could typically be obtained using a standard injection scheme. This was done by adjusting the parameters of a gamma variate function combined with a dispersion term to resemble the averaged arterial bolus size and shape observed around large vessels in six normal volunteers participating in clinical testing (27) of Sprodiamide (Nycomed Inc., Princeton, NJ, and Nycomed Imaging AS, Oslo, Norway). The resulting analytical expression was:

$$C_a(t) \propto \begin{cases} 0 & t \leq t_0 \\ (t - t_0)^{3.0} \cdot e^{-\frac{t}{1.5s}} & t > t_0 \end{cases} \quad [19]$$

where t_0 is the tracer arrival time. The subsequent recirculation was modeled to have a delay of 8 s and a dispersion with a time constant of 30 s. This was achieved

by convolving the gamma variate with an exponential with these time constants.

Simulated Tissue Signal

To test how well the deconvolution techniques reproduce the shapes and initial heights of $F_t \cdot R(t)$ in Eq. [6] we applied them to cases of known residue functions $R(t)$. These were chosen to represent extremes of potential residue shapes to test the robustness of the deconvolution techniques applied. We used three different models for the tissue residue function:

Box-shaped

This residue function is described by

$$R(t) = \begin{cases} 1 & t \leq \text{MTT} \\ 0 & t > \text{MTT} \end{cases}$$

This residue function describes a vascular bed with “plug” flow where the capillaries are in parallel with equal length and mean transit times.

Triangle

The residue function is in this case described by

$$R(t) = \begin{cases} 1 - \frac{t}{2 \cdot \text{MTT}} & t \leq 2 \cdot \text{MTT} \\ 0 & t > 2 \cdot \text{MTT} \end{cases}$$

Exponential

This residue function is described by

$$R(t) = e^{-\frac{t}{\text{MTT}}}$$

As mentioned above, this residue function describes the vasculature as a single, well-mixed compartment.

C_{VOI} was calculated with $TR = 1000$ ms by Eq. [5] for range of CBV values ranging from 1–5%. Combinations of CBF in the range 10–60 ml/100 ml/min and MTT in the range 2–12 s were chosen to yield the corresponding CBV. In the following, we describe how these time concentration curves were converted into dynamic MRI signal time curves.

Throughout our simulations, tissue and arterial tracer levels were assumed to be measured by observing the susceptibility effect due to compartmentalized paramagnetic tracer (28). We used the linear relationship between vascular concentration of paramagnetic contrast agent and the observed susceptibility contrast (29, 30). The tissue concentration time curves were consequently converted into signal enhancement using the relation

$$S(t) = S_0 e^{-k \cdot C_{\text{VOI}}(t) \cdot TE} \quad [20]$$

with $C_{\text{VOI}}(t)$ from Eq. [5] and where S_0 is the baseline signal intensity and k a constant dependent on the relationship between the susceptibility effects and paramagnetic contrast agent concentration in tissue and around arteries. The constant k was fixed by matching a typical peak drop in signal intensity in white matter (17% in our perfusion protocol with a typical contrast agent dose) to the simulated peak signal drop at a full blood flow of 20 ml/100 ml/min assuming a box-shaped residue function and an MTT of 4 s, a typical finding in our clinical

studies (31). This corresponds to a full blood volume of 2.0% in white matter as observed by our spin-echo sequence. This is roughly 40% of the actual full blood volume of white matter (32), due to the sensitivity of the spin-echo sequence to very small vessels (30). S_0 was set to the typical baseline intensity of brain tissue. Simulated signal time curves (Eq. [20]) were generated in the form of images, and Gaussian noise was added to generate a SNR between 5 and 1000. For typical clinical dynamic imaging, SNR is in the lower end of this range, with single pixel SNR typically varying between 8 and 10. Before analysis, a 3 by 3 uniform smoothing kernel was applied to mimic the approach used in actual image analysis. For each combination of parameters, 1024 simulations were performed.

Small delays between the bolus arrival in the artery and the peripheral tissue may occur. Delays can be corrected using analytical techniques by introducing and subsequently fitting a delay in the expression describing the convolution in Eq. [6]. In the case of nonparametric deconvolution, this is less straight forward. Although in the absence of noise, these techniques should theoretically yield zero elements for $R(t)$ until the arrival of the bolus, this is not generally the case in the presence of noise. We consequently simulated the effects of these delays on the fitted flow values by temporally shifting the arterial input relative to the simulated signal time curves.

Optimization of Nonparametric Deconvolution Techniques

Before using the SVD and regularization deconvolution technique, the corresponding free parameters P_{SVD} and P_{REG} had to be optimized at a given SNR. This was done by determining the choice of these parameters that empirically yielded the best reproduction of F_t and $R(t)$ at a set of standard conditions. In all subsequent simulations, the parameters were then kept fixed at this value. We chose the standard conditions to be a MTT of 2 and 4 s and flows of 20 and 40 ml/100 ml/min with underlying triangular, box-shaped and exponential residue functions, respectively. For these 12 physiological conditions, theoretical signal time curves were generated in the form of synthetic images. Noise was subsequently added to yield the specified SNR to optimize P_{SVD} and P_{REG} . After addition of noise, nonparametric deconvolution was performed using SVD and regularization.

For every map, the average and standard deviation of F_t and the chi-square of the fit of the experimentally determined (deconvolved) $R(t)$ to the underlying “true” $R(t)$ (triangle, box, or exponential) was determined. The choice of free parameter (P_{REG} and P_{SVD} , respectively) that optimized the fit of $R(t)$ and minimized the difference between the fitted and actual flow simultaneously for all combinations of MTT and CBF and underlying residue functions was subsequently chosen. In cases where a large range of choices of P_{SVD} and P_{REG} reproduced correct flow, the choice that minimized the standard deviation of F_t was chosen. In some cases, no choice of P_{SVD} and P_{REG} reproduced F_t and $R(t)$ well for all choices of residue functions and hemodynamic parameters simul-

taneously. The choice that brought the average F_t as close as possible to the actual value was then chosen.

The optimization of the FT approach was chosen according to the simulations of Gobbel and Fike (7). Their simulations showed that a choice of 0.1 for their *oscillatory index* was optimal to reproduce flow at different volumes and MTTs for nonpermeable vessels. This choice was consequently used in our simulations.

RESULTS

In the following, we describe our simulation results in two main sections: In the first, we describe the reproduction of flow for model-dependent and model-independent deconvolution techniques. In the second, we describe the capability of model-independent deconvolution techniques to determine the shape of the residue function $R(t)$.

Estimates of F_t

Figure 1 summarizes the estimates of flow for all four deconvolution techniques for high SNR (150) and low SNR (10) for different underlying residue functions. In all cases, the vascular volume was kept constant at 3.0%. Subsequently, we discuss the dependence of F_t on the underlying vascular volume.

Model-Dependent Deconvolution. Model-dependent deconvolution yielded a good estimate of absolute flow when the underlying (true) residue function is described by the chosen function, in this case an exponential (See Fig. 1a). For other underlying residue models, fitted flow was still proportional to the actual flow rate and the approach will consequently yield correct *relative* flow values if the shape of the residue function is uniform across the brain. In comparing regions with different residue functions, however, even relative flow values could be in substantial error. Note, for example, that, assuming an exponential residue model, an area with a triangular or box-shaped residue function will have the same fitted flow rate as that of an area with a "true" exponential residue function but 50% higher actual flow.

Model-Independent Deconvolution. The FT (Figs. 1c and 1d) approach yielded reasonable estimates of F_t for low flow rates at both high and low SNR. However, we found F_t to be substantially underestimated at high flow rates. This effect was somewhat worse at low SNR compared with higher SNR. We found the underestimation to be an effect of short MTTs (2–3 s) at the high flow rates in Figs. 1c and 1d. The estimate of F_t was thus improved when it was associated with a longer MTT (results not shown). The flow estimates all showed some dependency on the underlying residue function. We will discuss this failure to reproduce flow at short MTTs and the dependency on underlying residue function in greater detail below.

The regularization approach (Figs. 1e and 1f) yielded good reproduction of F_t over a wide range of flow values with only a slight dependence on the underlying residue model. The dependence on the underlying residue function was far smaller than that of the model-dependent approach. Also, notice that standard deviations at each point are only slightly larger than those of the model-dependent, analytical deconvolution. There is some overestimation of absolute flow values using this deconvolution technique, especially for low flow values.

The SVD approach (Figs. 1g and 1h) also yielded reproduction of flow relatively independent of the underlying residue function. In this case, fitted flow tends to be somewhat underestimated at high flow rates. The standard deviations at each point are about 10–15% of the absolute value, somewhat lower than the corresponding values for the regularization approach.

Figure 2 shows results of a set of simulations similar to those shown above at low SNR (10) for the regularization and SVD deconvolution techniques at a higher vascular volume (4.5%). For the regularization approach (Fig. 2a), the change in volume results in a large change in fitted flow, especially in case of an underlying box shaped residue model. We discuss the cause of this change in the section below. For the SVD technique (Fig. 2b), fitted flow values remain relatively constant with a tendency for high flow rates to be less underestimated than in Fig. 1h at the higher vascular volume. This is probably a result of the better definition of the bolus shape relative to the underlying noise due to the larger vascular volume.

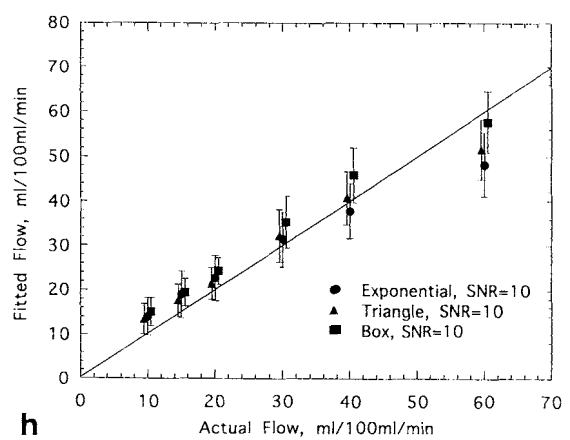
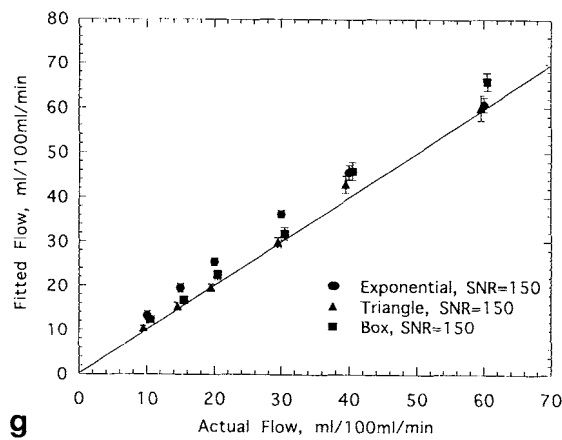
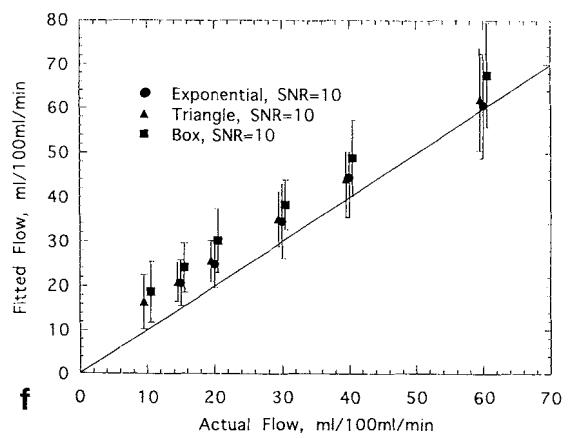
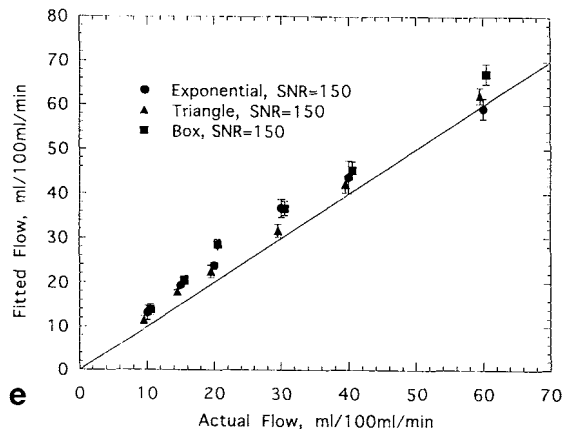
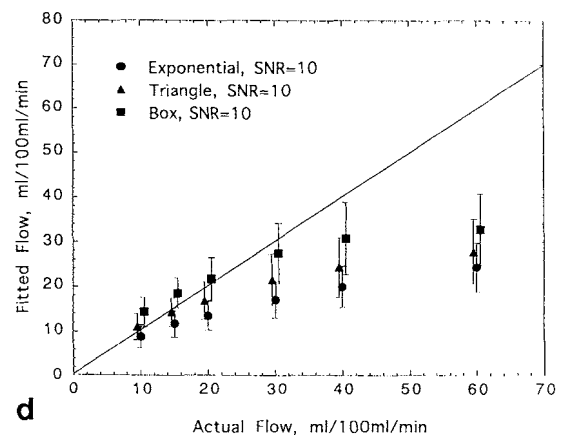
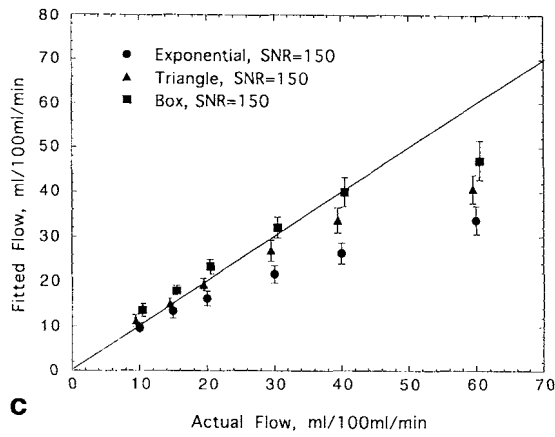
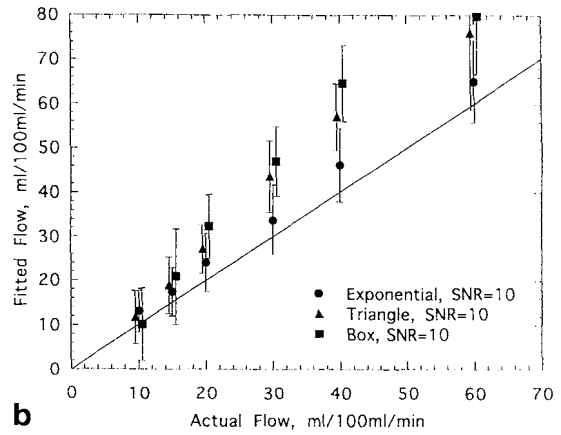
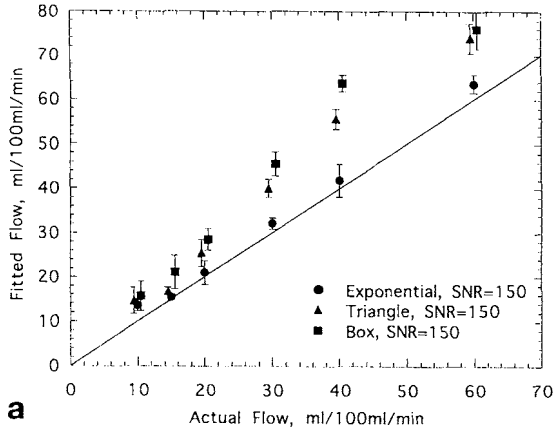
Table 1 summarizes the simulation results. Figure 3 shows the effect of a 2-s delay of the measured tissue signal relative to the arterial input on the fitted flow rates using SVD. Note that, as flow rates increase, fitted flow values become increasingly underestimated. However, flow values are less sensitive to delays when assessing flow values less than 20 ml/100 ml/min.

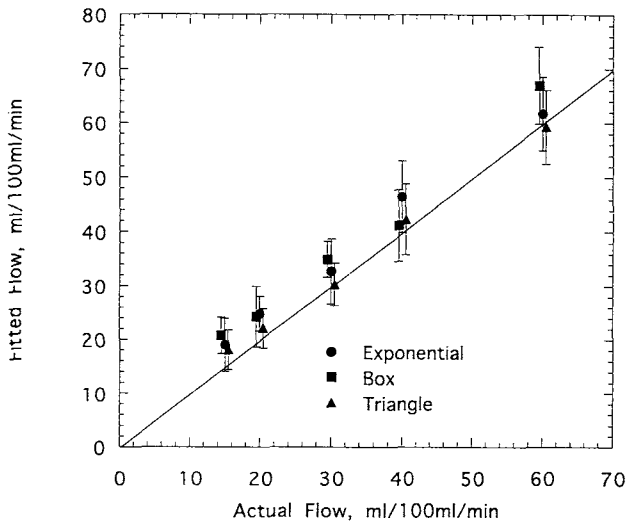
Reproduction of $R(t)$

Figures 4a and 4b show the shape of the residue function determined using SVD and regularization. The underlying residue function was a box with MTT = 12 s and tissue flow 10 ml/100 ml/min. Means of 1024 simulations are shown. This example was chosen for the purpose of illustration. The conclusions were, however, valid for other combinations of F_t . The standard deviation at each point of the curve was generally about 10% of the absolute value for SNR = 150 and 40% of the absolute value for SNR = 10.

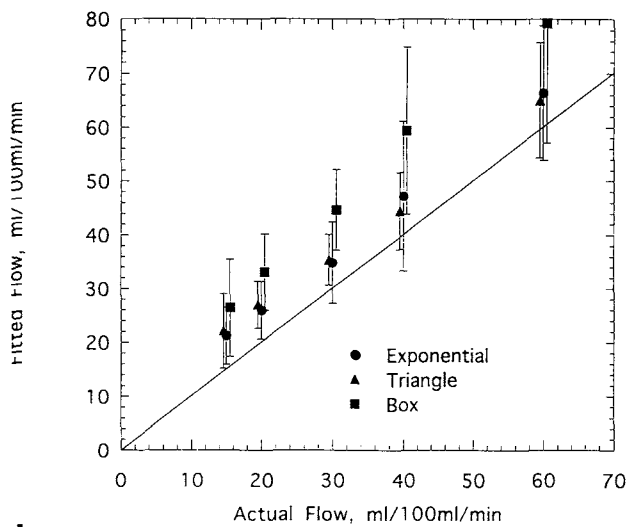
For the SVD approach (Fig. 4a), note that the shape of the residue function becomes less detailed with decreasing SNR. The initial and maximum points on the reproduced residue curves, however, still remains constant. It

FIG. 1. Reproduction of flow using model-dependent fitting (exponential residue model) and model-independent deconvolution (FT, regularization, and SVD) with different underlying residue functions. SNRs were for each technique 150 and 10, respectively, and the CBV 3%. (a) and (b) show model-dependent fitting of flow using an exponential residue model. Note how the resulting flow is heavily dependent on the underlying residue function except when the underlying residue function is described by the chosen model. (c) and (d) show the same simulation scheme for the FT at SNR = 150 and SNR = 10. Note that flow is poorly reproduced. For the regularization approach ((e) shows SNR = 150 and (f) SNR = 10) and the SVD ((g) is again SNR = 150 and (h) SNR = 10) reproduction of flow is relatively independent of the underlying residue function. The SVD somewhat underestimates high flow values. Error bars indicate 1 SE.





a



b

FIG. 2. Reproduction of flow values for different underlying residue functions for the regularization (a) and SVD (b) approaches, respectively, at SNR = 10. In this case, vascular volume was 4.5%. Note that the flows fitted by regularization approach show a strong dependence on CBV, whereas this was less prominent with the SVD approach (compare with Figs. 1f and 1h). The high flow values seem to be less underestimated at this volume than in the case of a CBV of 3.0% (Fig. 1h).

Table 1
Summary of Monte Carlo Modeling Results

Deconvolution approach	Flow estimate independence of		
	Vascular structure	CBF	CBV
Model dependent (exponential)	÷		
Fourier transform	+	÷	
Regularization	+	+	÷
SVD	+	+	+

Flow estimate independence of a given quantity is indicated by +, dependence by ÷.

was a general finding of our simulations that there was no sudden loss of the degree to which the fitted curves reflected the underlying true residue function. Rather, the shape changed from that of the true underlying residue function to a smooth curve with only few of the details of the underlying residue function.

The regularization approach (Fig. 4b) generally showed a tendency to change the fitted residue function into a triangular shape when going toward lower SNR. This is probably due to the constraint imposed by the regularization term, favoring this shape. Also, each point of the fitted $R(t)$ was determined with increased uncertainty at the lower SNR. We believe this bias toward a triangular shape is the cause of the overestimation of flow noticed for regularization approach in Fig. 2a.

Generally, using the SVD, at a SNR of below 50–100, the noise on each point on the determined underlying residue function was too large to yield qualitative information on the underlying curve. For the regularization approach, higher SNR was found to be necessary to determine the shape of the residue function.

DISCUSSION

Our simulations clearly demonstrate the potential dangers of using simplified assumptions when modeling the vascular residue function. Assuming a simple, mono-exponential residue function will thus introduce large systematic errors when flows in two regions with different residue functions are compared. This is in line with the conclusions made by Lassen (10) and Weisskoff *et al.* (12). We performed simulations to evaluate if using a multi-exponential residue model improved the reproduction of flow. The introduction of extra parameters, however, did not change this general conclusion. This result is a drawback to the choice of the exponential as a first approximation to the residue function in the model-dependent approach. In a companion paper (31), we qualitatively analyze other simple, analytical expres-

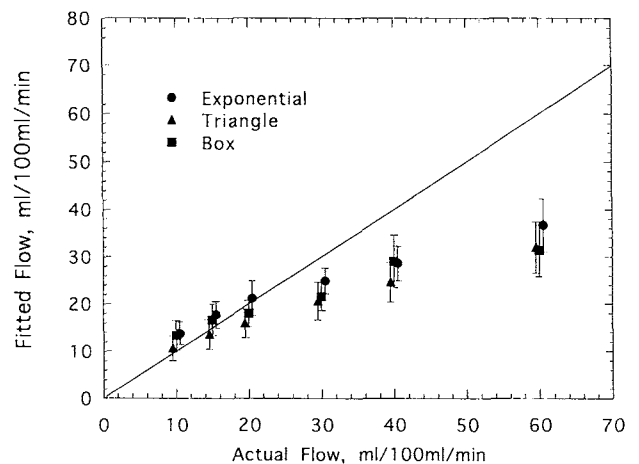


FIG. 3. Reproduction of flow at a CBV of 3.0% and the SVD model-independent deconvolution approach. The tissue concentration time curve was delayed by 2 s relative to the arterial input. Note how this causes substantial underestimation of flow at high flow values, whereas low flow rates are still well reproduced.

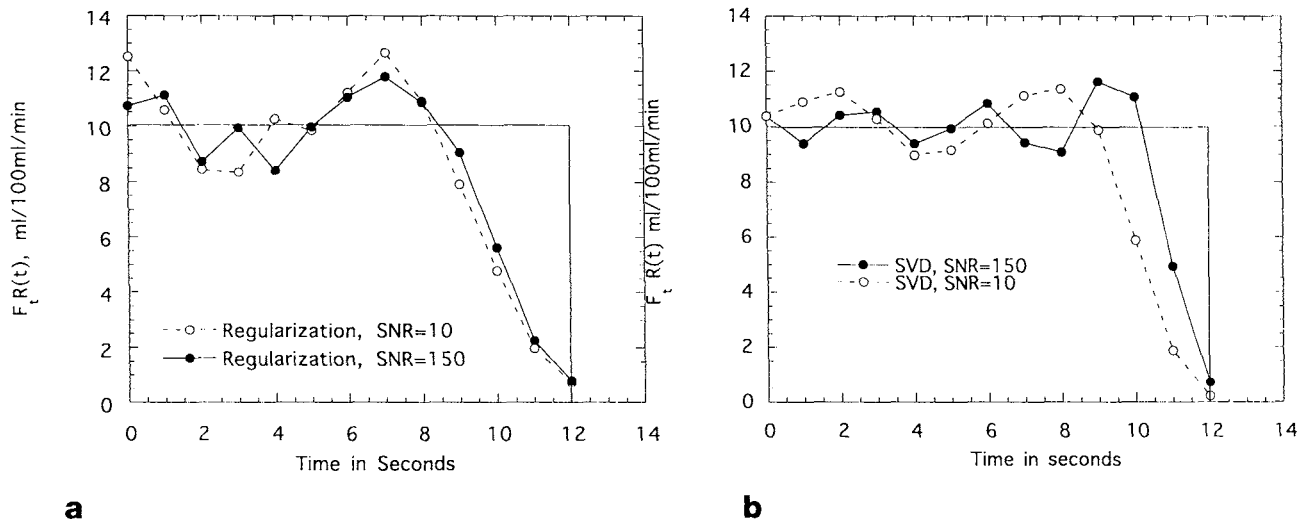


FIG. 4. (a) Optimized reproduction of the underlying residue function for the SVD nonparametric deconvolution technique at two different noise levels, SNR = 150 and SNR = 10. The solid line indicates the true, underlying residue function. Note that the shape gradually loses resemblance to the underlying residue function going toward lower SNR. CBV was 3.0%. (b) Optimized reproduction of the underlying residue function for the regularization nonparametric deconvolution technique at two different noise levels, SNR = 150 and SNR = 10. The solid line indicates the true, underlying residue function. Note that the shape tends to become more triangular as the SNR decreases, reflecting the underlying regularization term. CBV was 3.0%.

sions to characterize the cerebral residue function. Models including very detailed models of vascular transport and exchange have been proposed (33). Further work is needed to provide operators that describe a wide variety of vascular residue functions in the brain.

Of nonparametric deconvolution techniques evaluated, the Fourier transform failed to reproduce F_t at short MTTs just as it showed a dependency on the underlying residue function. These facts are both reflections of the properties of the FT in the physiological context in which we applied it. Even in the absence of noise, the FT gives approximately $F_t/2$ at the initial point of the response function. The flow is thus estimated from the following point on the response curve. This has two effects. First, for relatively short MTTs compared with the sampling rate, the impulse response function will have decayed substantially at the first sample of the residue function, leading to underestimation of flow as we found in our simulations. Secondly, the degree of decay of the response function before the second sample is dependent on the residue model. In agreement with this, flow was most severely underestimated for the most rapidly decreasing residue model, namely the exponential. Furthermore, applying filters to improve the SNR of the measurement introduces a blurring in the time domain, causing the maximum point on the response curve to be further underestimated. This was demonstrated in our simulations by the more severe underestimation of flow at low SNR where more powerful filtering had been applied.

The underestimation of flow for short MTTs relative to the sampling rate has severe implications for determination of flow using FT. In comparing two regions with equal actual flow, the region with the highest CBV (and thus longest MTT) will appear to have a higher flow rate using the FT, making the estimates biased by the rCBV. The FT approach is thus misleading in evaluating states

of high flow and short MTT unless the sampling rate can be improved relative to the MTTs in question. Interestingly, the use of an unmodified Wiener filter, may not be optimal in finding residue functions. The Wiener filter is designed to minimize the mean square error over all time whereas we, for estimates of flow, wish to minimize the errors in just the initial value of the residue function. Because of these differences, the use of a true Wiener filter would produce large underestimations flow. In light of these theoretical concerns, we compared simulation results obtained with the modified Wiener filter (6) to similar results obtained with a Hanning filter after optimization to yield similar standard deviations of the flow estimates. We got comparable reproduction of flow rates for the two approaches, demonstrating that the modifications to the Wiener filter approach by Gobbel *et al* (6) compensate for the theoretical draw-backs mentioned above.

Nonparametric deconvolution using regularization could be optimized to yield good reproduction of flow. However, subsequent use of the technique at a different rCBV showed some dependence on vascular volume. We believe this effect should be seen as a result of the fact that changing CBV effectively changes the SNR of the concentration time curve. Since the optimization of the regularization is dependent on the SNR, one choice of this optimization may not suffice to optimize the reproduction of flow for all values of CBV, thus introducing the observed bias on flow rates. More optimal regularization terms than the one we used here may improve this technique.

The SVD nonparametric deconvolution technique—in contrast to the other model-independent approaches—showed an excellent ability to reproduce flow with good accuracy independent of the underlying vascular structure and volume. The bias of underlying residue function increased somewhat toward combinations of high flow

and short MTT. This should probably be seen as a reflection of the fact that linear approximation to the underlying residue function between measurements assumed in this approach is poor under these conditions. This bias can be minimized by improving temporal resolution of the imaging sequence, making the linear approximation between measured points better. Also, the elements in the convolution matrix (Eq. [8]) can be further modified to produce a smoother interpolation of the residue function between measured points. The SVD nonparametric deconvolution thus shows good promise as a nonparametric deconvolution technique for bolus passage studies in the brain.

For all deconvolution techniques, flow estimates became more uncertain toward shorter MTT. This is an effect of the arterial input varying slowly compared with MTT, the characteristic time scale of the residue function that we want to sample. Note that the characteristic time scale of the arterial input used in our simulations is roughly 1.5 s (Eq. [19]). This general constraint can only be circumvented by using rapid bolus injections to create very sharp arterial input profiles.

The ability of nonparametric deconvolution techniques to reproduce the *shape* underlying residue function $R(t)$ was generally poorer than the ability to reproduce flow. Model-independent approaches in our simulations required high SNR (50–100 with a typical contrast injection, imaging sequence and resolution in the brain) to reproduce the tissue residue function. This should be compared with the pixel-by-pixel SNR of about 10 in our actual imaging experiments. Performing regional rather than pixel-by-pixel deconvolution will thus still provide mostly qualitative information on the shape of the residue function just as tissue heterogeneity will cause a loss of specific, localized information. This technique thus awaits the development of more potent contrast agents and ways of obtaining higher SNR in human studies of $R(t)$. In an experimental setting, however, animal experiments at high field using iron oxide contrast agents may provide sufficient SNR and contrast-to-noise ratio (CNR) to allow high resolution studies of $R(t)$ with this technique. This may, in turn, provide important information on vascular structure and reactivity in normal as well as pathological brain tissue.

Our analysis shows that delays between arterial input and the tissue response are important in accurately determining flow. It is important to note that tracer arrival delays often occurs in states where flow is low, for example as a result of collateral circulation in the periphery of stroke areas. In these situations, our simulations indicate that flow will only be slightly underestimated. In regions of high flow, high flow rate in the afferent vessels will tend to create a relatively shorter delay. On the other hand, underestimation of tissue flow were shown to be more severe, and delays should consequently be corrected during image analysis by either fitting the delay as a free parameter (model-dependent approach) or independent determination of the tracer arrival delays (model-independent approaches). We are presently investigating methods for performing this correction. Also, it should be noted that the pathologies mentioned above are examples where dispersion of the arterial input func-

tion could potentially take place. Again, this dispersion will be dependent on the flow rate in the afferent vessels and thus on tissue flow. Correction for vascular dispersion requires specific models for vascular transport and is the subject of on-going research (33).

CONCLUSION

We have performed Monte Carlo simulations to test the ability of analytical (model-independent) as well as nonparametric (model-dependent) deconvolution techniques to reproduce flow in MRI bolus experiments at a range of SNRs. The use of model-dependent approaches may lead to large systematic error in comparing regions with different residue function.

The model-independent approaches allowed good reproduction of the true, underlying vascular residue function only at high SNR. Toward lower SNR, the fitted residue functions were in mere qualitative agreement with the actual, underlying residue function.

We demonstrated that SVD is able to reproduce flow with good accuracy relatively independent of the underlying vascular structure even at the SNR typical of pixel-by-pixel deconvolution after 3-by-3 uniform filtering of the images. This approach thus shows promise as an approach to high resolution model-independent determination of CBF using dynamic imaging of paramagnetic bolus passages in humans.

REFERENCES

1. G. N. Stewart, Researches on the circulation time in organs and on the influences which affect it. Parts I-III. *J. Physiol. (London)* **15**, 1 (1894).
2. P. Meier, K. L. Zierler, On the theory of the indicator-dilution method for measurement of blood flow and volume. *Appl. Physiol* **6**, 731–744 (1954).
3. L. Axel, Cerebral blood flow determination by rapid-sequence computed tomography. *Radiology* **137**, 679–686 (1980).
4. B. R. Rosen, J. W. Belliveau, J. M. Vevea, T. J. Brady, Perfusion imaging with NMR contrast agents. *Magn. Reson. Med.* **14**, 249–265 (1990).
5. B. R. Rosen, J. W. Belliveau, B. R. Buchbinder, R. C. McKinstry, L. M. Porkka, D. N. Kennedy, M. S. Neuder, C. R. Fisel, H. J. Aronen, K. K. Kwong, R. M. Weisskoff, M. S. Cohen, T. J. Brady, Contrast agent and cerebral hemodynamics. *Magn. Reson. Med.* **19**, 285–292 (1991).
6. G. T. Gobbel, C. E. Cann, J. R. Fike, Measurement of regional cerebral blood flow using ultrafast computed tomography. Theoretical aspects. *Stroke* **22**, 768–771 (1991).
7. G. T. Gobbel, J. R. Fike, A deconvolution method for evaluating indicator-dilution curves. *Phys. Med. Biol.* **39**, 1833–1854 (1994).
8. K. A. Rempp, G. Brix, F. Wenz, C. R. Becker, F. Guckel, W. J. Lorenz, Quantification of regional cerebral blood flow and volume with dynamic susceptibility contrast-enhanced MR imaging. *Radiology* **193**, 637–641 (1994).
9. N. Wilke, K. Kroll, H. Merkle, Y. Wang, Y. Ishibashi, Y. Xu, J. Zhang, M. Jerosch-Herold, A. Mühler, A. E. Stillman, J. B. Bassingthwaite, R. Bache, K. Ugurbil, Regional myocardial blood volume and flow: first-pass MR-imaging with polylysine-Gd-DTPA. *J. Magn. Reson. Imaging* **5**, 227–237.
10. N. A. Lassen, Cerebral transit of an intravascular tracer may allow measurement of regional blood volume but not regional flow. *J. Cereb. Blood Flow Metabol.* **4**, 633–634 (1984).
11. J. A. Jacquez, in "Compartmental Analysis in Biology and Medicine. Kinetics of distribution of tracer-labeled materials," pp. 84–101, Elsevier Publishing Company, Amsterdam, 1972.
12. R. M. Weisskoff, D. Chesler, J. L. Boxerman, B. R. Rosen, Pitfalls in MR measurements of tissue blood flow with intravascular tracers: which mean transit time? *Magn. Reson. Med.* **29**, 553–559 (1993).

13. O. A. Larsen, N. A. Lassen, Cerebral haematocrit in normal man. *J. Appl. Physiol.* **19**(4), 571–574 (1964).
14. G. M. Wing, in "A Primer on Integral Equations of the First Kind. The Problem of Deconvolution and Unfolding." SIAM Publishing Company, Santa Fe, NM, 1991.
15. W. H. Press, S. A. Teukolsky, W. T. Vetterling, B. T. Flannery, in "Numerical Recipes in C. The Art of Scientific Computing," 2nd ed., Cambridge University Press, Oxford, 1992.
16. J. B. Bassingthwaighe, C. A. Goresky, in "Handbook of Physiology Section 2: The Cardiovascular System" (E. M. Renkin, C. G. Michel, Eds.), pp. 549–626, American Physiology Society, Bethesda, 1984.
17. N. A. Lassen, O. Henriksen, P. Sejrsen, in "Handbook of Physiology Section 2: The Cardiovascular System" (J. T. Shepherd, F. M. Abboud, Eds.), pp. 21–64, American Physiology Society, Bethesda, 1984.
18. C. M. Coulam, H. R. Warner, H. W. Marshall, J. B. Bassingthwaighe, A steady-state transfer function analysis of portions of the circulatory system using indicator dilution techniques. *Comput. Biomed. Res.* **1**, 124–138 (1967).
19. C. M. Coulam, H. R. Warner, E. H. Wood, J. B. Bassingthwaighe, A Transfer function analysis of coronary and renal circulation calculated from upstream and downstream indicator-dilution curves. *Circ. Res.* **19**, 879–890 (1966).
20. C. I. I. Wall, H. S. Borovetz, J. J. Murphy, R. L. Hardesty, System parameter identification in transport models using the fast Fourier transform (FFT). *Comput. Biomed. Res.* **14**, 570–581 (1981).
21. J. B. Bassingthwaighe, Blood flow and diffusion through mammalian organs. *Science* **167**, 1347–1353 (1970).
22. M. E. Valentinuzzi, E. M. M. Volachec, Discrete deconvolution. *Med. Biol. Eng.* **13**, 123–125 (1975).
23. A. Todd-Pokropek, in "Cerebral Blood Flow. Mathematical Models, Instrumentation, and Imaging Techniques" (A. Rescigno, A. Boicelli, Eds.), pp. 107–119, Plenum Press, New York, 1988.
24. T. A. Bronikowski, C. A. Dawson, J. H. Linehan, Model-free deconvolution techniques for estimating vascular transport functions. *Int. J. Biomed. Comput.* **14**, 411–429 (1983).
25. J. Bock, P. Deuflhard, A. Hoefft, H. Korb, H.-G. Wolpers, J. Steinman, G. Hellige, Thermal recovery after passage of the pulmonary circulation of the pulmonary circulation assessed by deconvolution. *J. Appl. Physiol.* **64**, 1210–1216 (1988).
26. S. Van Huffel, J. Vandewalle, M. C. De Roo, J. L. Willems, Reliable and efficient deconvolution technique based on total linear least squares for calculating the renal retention function. *Med. Biol. Eng. Comput.* **25**, 26–33 (1987).
27. A. G. Sorensen, S. M. Kulke, R. M. Weisskoff, J. L. Boxerman, B. R. Buchbinder, B. R. Rosen, Investigation of cerebral hemodynamics with spirodiamide (Dy-DTPA-BMA) and functional magnetic resonance imaging, in "Proc., ASNR, Nashville, 1994", p. 237.
28. A. Villringer, B. R. Rosen, J. W. Belliveau, J. L. Ackerman, R. B. Lauffer, R. B. Buxton, Y.-S. Chao, V. J. Wedeen, T. J. Brady, Dynamic imaging with lanthanide chelates in normal brain: contrast due to magnetic susceptibility effects. *Magn. Reson. Med.* **6**, 164–174 (1988).
29. R. M. Weisskoff, C. S. Zuo, J. L. Boxerman, B. R. Rosen BR, Microscopic susceptibility variation and transverse relaxation: theory and experiment. *Magn. Reson. Med.* **31**, 601–610 (1994).
30. C. R. Fisel, J. L. Ackerman, R. B. Buxton, L. Garrido, J. W. Belliveau, B. R. B. R. Rosen, T. J. Brady, MR contrast due to microscopically heterogeneous magnetic susceptibility: numerical simulations and applications to cerebral physiology. *Magn. Reson. Med.* **17**, 348–356 (1991).
31. L. Østergaard, A. G. Sorensen, K. K. Kwong, R. M. Weisskoff, C. Gyldensted, B. R. Rosen. High resolution measurement of cerebral blood flow using intravascular tracer bolus passages. Part II: Experimental comparison and preliminary results. *Magn. Reson. Med.* **36**, 726–736 (1996).
32. K. L. Leenders, D. Perani, A. A. Lammertsma, J. D. Heather, P. Buckingham, J. R. Healy, J. M. Gibbs, R. J. S. Wise, Y. Hatazawa, S. Herold, R. P. Beany, D. J. Brooks, T. Spinks, C. Rhodes, R. S. J. Frackowiak, T. Jones, Cerebral blood flow, blood volume and oxygen utilization: normal values and effect of age. *Brain* **113**, 27–47 (1990).
33. J. B. Bassingthwaighe, I. S.J Chan, C. Y. Wang, Computationally efficient algorithms for convection-permeation-diffusion models for blood-tissue exchange. *Ann. Biomed. Eng.* **20**, 687–725 (1992).